Towards Inline Optical Assessment of Fiber-Web Uniformity Using Robust Image-Based Algorithms

A Simulation Benchmark and an Industrial Image Study

Sebastian Geldhäuser[1], Felix Andrew Herbst[2], Alexandra Teynor[2], Maximilian Wohlschläger[3], Raphael Weiss[3], Mesut Cetin[1,2]

[1]Institut für Textiltechnik Augsburg gGmbH, [2]Technische Hochschule Augsburg, [3]Dr. Schenk GmbH Industriemesstechnik

sebastian.geldhaeuser@ita-augsburg.de

Background, Aim & Approach

Background & Aim

Carded fiber webs are the starting point for many nonwoven products, and every downstream step inherits the mass distribution produced by the card [1]. Optical line-scan inspection covers the full web width; under fixed illumination, optics and material, gray value serves as a proxy for local material distribution [2, 3]. Numerous image-based uniformity indices exist, yet none has been agreed upon [4–6]. Moll et al. favored the coefficient of variation (CV) for fiber injection molded preforms [6], but a carded web imaged from above on a dark conveyor differs in fiber organization, contrast and geometry. This study examines whether that recommendation transfers and what a multi-scale measure adds.

Four Quadrat-Based Measures

	Single grid 40 × 40 cells		Aggregated over 39 grids 2 × 2, 3 × 3, … , 40 × 40
Gray values	**CV** $\mathrm{CV} = \frac{s}{\bar{q}}$ *std. dev. / mean*	**Index of dispersion** $I_\mathrm{d} = \frac{s^2}{\bar{q}}$ *variance / mean*	**Gray-value chi-square [4]** $T_i = i^2 \bar{q}_i \mathrm{CV}_i^2 \quad \mathrm{UI} = \frac{100}{1+R}$ *stages integrated vs. 97.5 % χ^2 reference*
Binarized (area fraction)	*not part of the comparison*		**Binary chi-square [3]** $T_i^{\mathrm{bin}} = i^2 \bar{f}_i \mathrm{CV}_{f,i}^2 \quad \mathrm{UI}_{\mathrm{bin}} = 100\left(1 - \frac{\Sigma T_i^{\mathrm{bin}}}{\Sigma \mathrm{df}_i}\right)$

Fig. 1. The four measures span three design decisions: single grid vs. aggregation over grids, gray values vs. binarization, and normalization by the mean vs. the variance-to-mean ratio.

All four measures evaluate the dispersion of the cell means q_j on equal-area cells (Fig. 1). Gray-value chi-square combines the stage statistics T_i of all grids into $\mathrm{UI} = 100/(1+R)$, with R the integral of T_i over the degrees of freedom normalized by that of the 97.5 % chi-square reference; binary chi-square relates the summed T_i to the summed degrees of freedom. Larger scores indicate greater uniformity, whereas for CV and I_d smaller values do.
Since $I_\mathrm{d} = \mathrm{CV}^2 \cdot \bar{q}$, the index of dispersion adds no independent spatial information; on the 40 × 40 grid it is proportional to the finest chi-square stage and thus isolates the effect of scale aggregation.

Research Questions

- **Q1** How finely do the four measures separate controlled structural states, and how strongly do they depend on block averaging?
- **Q2** How closely do the retained measures agree when ranking production images within one basis-weight setting?
- **Q3** Where in the grid hierarchy do remaining disagreements arise, and do they matter relative to process variation?

Industrial Setup & Scale Selection

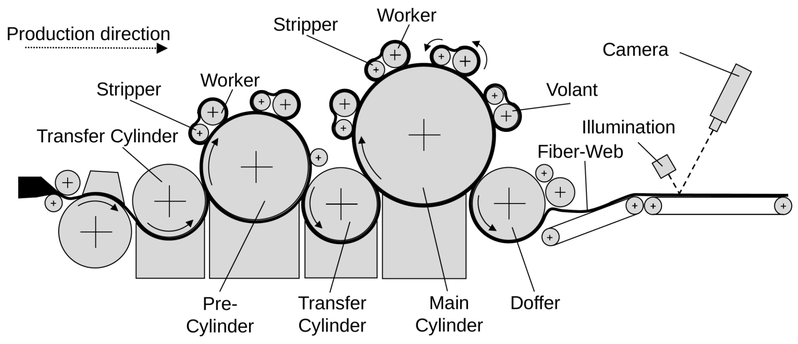


Fig. 2. Card layout and position of the inspection system above the conveyor.

The inspection system (Dr. Schenk GmbH, Gräfelfing, Germany) images the web of 3.3 dtex polyester fibers behind the doffer, with illumination and two double-line cameras above the web, so bright fibers appear against the dark conveyor. Instead of treating quadrat size as a free parameter, the acquisition chain fixes the finest grid: 32 × 32 block averaging turns a 1280 × 1280 px snapshot into a 40 × 40 matrix of 2.2 mm superpixels (Fig. 3).

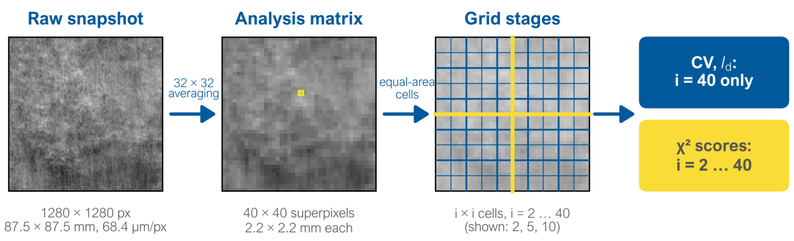


Fig. 3. Acquisition chain fixing the observation scale (production image from group G6).

Operating blocks comprise six images at settings unchanged for at least 120 s, grouped by calculated basis weight.

155	8	312	432
operating blocks	basis-weight groups	images in G6 (25.8 g/m²)	images in G4 (12.9 g/m²)

Results A: Simulation Benchmark

A1. Fiber-Resolved Web Simulation

Testing the measures requires images of known structure. Point-pattern references [3, 4, 6] differ strongly from production images, so a fiber-based simulation was developed that reproduces the real imaging situation as closely as possible [3, 4, 7]. In an image of width B, start points scatter around C_n cluster centers with $\sigma = \mathrm{CWF} \cdot B/\sqrt{C_n}$, so a small cluster width factor (CWF) concentrates material and a large one spreads it (Fig. 4a). Fibers are drawn as 30 mm random walks, their number follows a mass balance, and contrast was calibrated against production images; CWF (0.1–50) and C_n (16–1600) were varied.

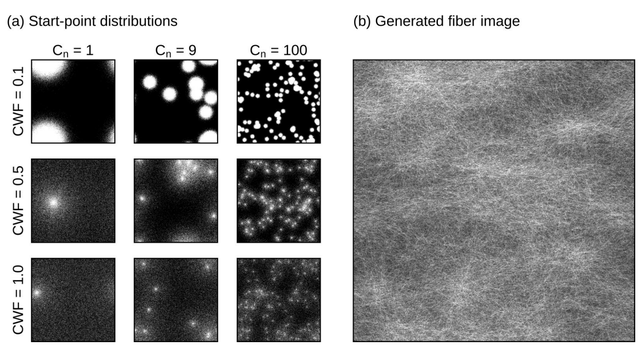


Fig. 4. (a) Start-point distributions for C_n = 1, 9, 100 and CWF = 0.1, 0.5, 1.0; (b) fiber image.

A blinded survey checked this similarity. Because industrial systems reduce the data volume by block averaging, images were shown at 40 × 40, 80 × 80 and 160 × 160 px and at full resolution; eleven participants judged 50 images per stage, half simulated (550 judgments per stage, 2,200 in total). Accuracy stayed near chance at 40 × 40 and 80 × 80 px (54 %, 51 %), rose slightly at 160 × 160 px (59 %) and reached 72 % only at full resolution, where fiber-level detail exposed the simulation, most readily for coarse clusters (Fig. 5).

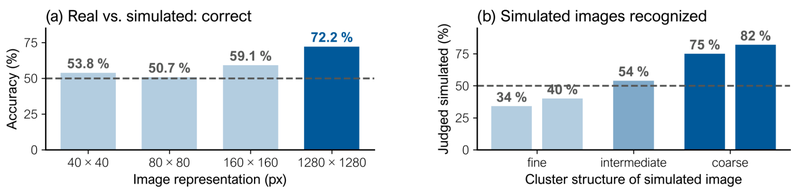


Fig. 5. Visual distinguishability: (a) accuracy per image representation; (b) recognition rate of simulated images per cluster structure, pooled over all four representations; dashed: 50 %.

A2. Response to Structural Change

All four measures follow the controlled change in the expected direction. As raw spans are not commensurable, the fair test is how far each separates two clearly different states: at C_n 16, CWF 0.1 and 1.0 distribute the same mass as sixteen tight spots or around sixteen centers. CV, I_d and gray-value chi-square render this clearly, whereas binary chi-square barely responds over the entire cluster range (Fig. 6).

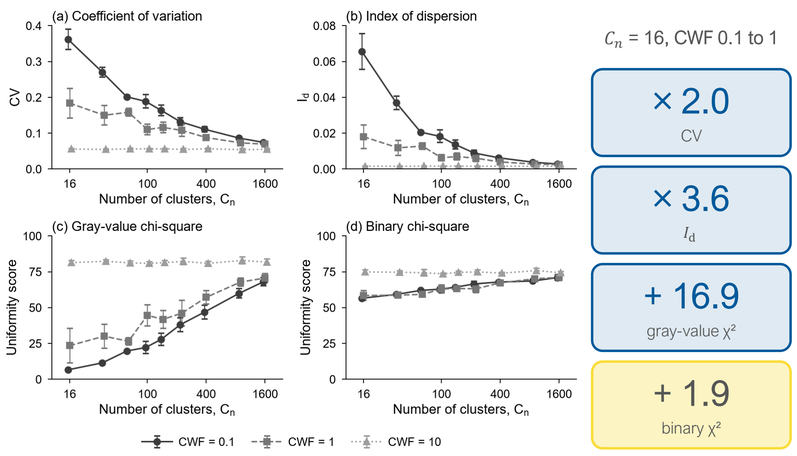


Fig. 6. Response to the number of clusters C_n at 30 g/m² for three CWF values (mean ± SD, five realizations); right: separation of the two states at C_n = 16.

A3. Effect of Block Averaging

Repeating the CWF series at four block-averaging stages separates the measures again: CV and I_d remain invariant, and gray-value chi-square keeps its curve shape while its plateau rises from about 79.5 to 84. Binary chi-square shifts most, because thresholding does not commute with averaging; at full resolution it appears saturated, at the operating stage it still responds (Fig. 7).

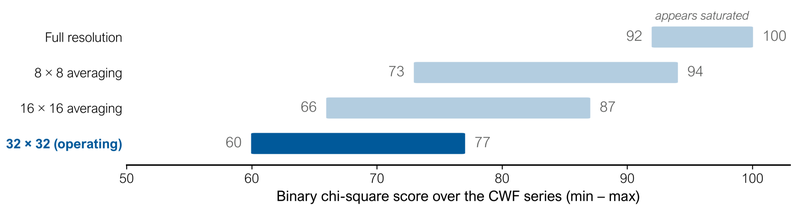


Fig. 7. Range of binary chi-square over the CWF series per block-averaging stage.

Consequence: CV and gray-value chi-square are retained as principal measures, I_d as a supplementary one; binary chi-square discriminates least and depends on the processing position.

Results B: Industrial Images

B1. Basis-Weight Dependence

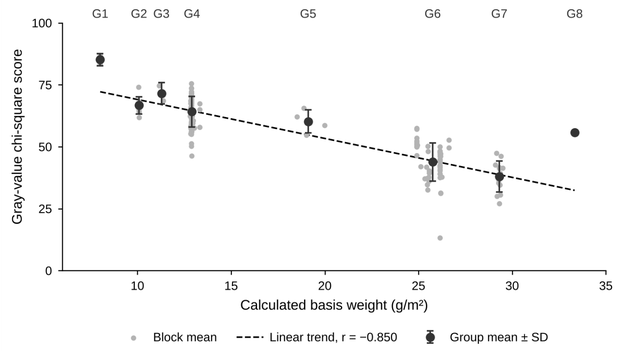


Fig. 8. Gray-value chi-square score versus calculated basis weight for 155 operating blocks with group means ± SD (G1–G8); right: Pearson r of each measure with basis weight.

Across all groups, the score decreases with calculated basis weight, and CV and I_d increase accordingly, whereas binary chi-square shows no trend (Fig. 8). The mean image level stays constant due to a correction in the inspection system, while the dispersion between cells grows. As the opposite trend has been reported under other acquisition conditions [8, 9], it is attributed to this inspection geometry; raw scores are compared only within one group.

B2. Rank Agreement within a Setting

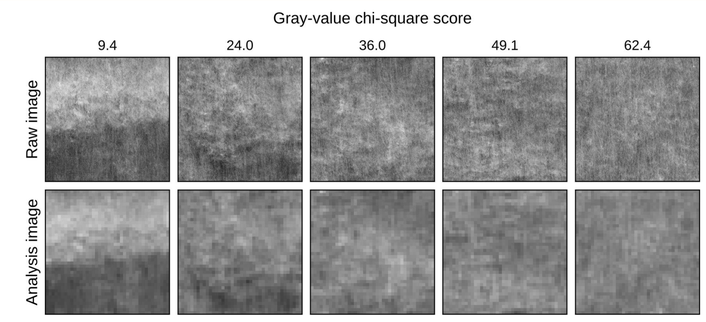


Fig. 9. G6 images across the score range; top: raw image, bottom: 40 × 40 analysis image.

Within G6, the score spans large bright and dark regions to a more even distribution with residual cloudiness (Fig. 9). Raw values relate nonlinearly, so differences cannot be transferred between indices, but percentile ranks align almost perfectly (Fig. 10), even more so in G4.

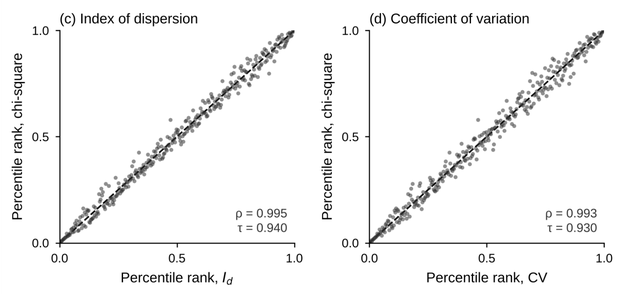


Fig. 10. Percentile ranks of I_d and CV versus gray-value chi-square in G6 (312 images); dashed: identical ranks.

B3. Where the Measures Disagree

The 3.5 % of G6 pairs that CV and gray-value chi-square order oppositely lie within 4.6 score points, below the scatter of 6.3 points under identical settings (Fig. 11). Decomposed into grid-stage contributions, the 40 × 40 grid favors one image, whereas stages 2 × 2 to 20 × 20 alone favor the other in 99.6 % of the pairs reversed between I_d and chi-square: aggregation over grids, not the chi-square form, causes the difference.

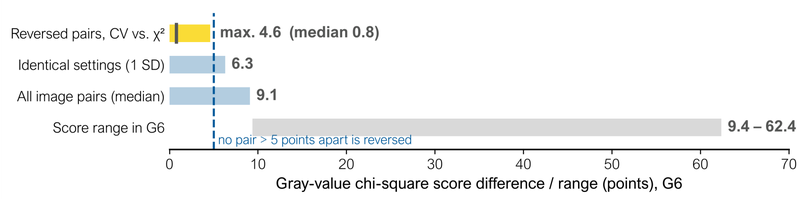


Fig. 11. Score differences of reversed pairs vs. process scatter and score range (G6).

Conclusion & Recommendation

Measure	Rating	Recommendation
CV	🟢	Primary indicator for routine monitoring
Gray-value χ²	🟢	Add where formations > 2.2 mm matter
Index of dispersion	🟡	Supplementary, mean-dependent
Binary χ²	🔴	Least discriminating, stage-dependent

CV transfers as the primary indicator: it ranks production images almost identically to gray-value chi-square and needs only one pass over the existing 40 × 40 matrix. Gray-value chi-square adds sensitivity to the arrangement of cell values, and its stage profile shows at which scale two images differ. The two-stage design offers a transferable procedure for selecting measures in new imaging situations.

Funded by

Bayerisches Staatsministerium für Wirtschaft, Landesentwicklung und Energie

[1] A.G. Brydon, A. Pourmohammadi, "Dry-laid web formation," in S.J. Russell (ed.), Handbook of Nonwovens, Woodhead Publishing, Cambridge, 2007, pp. 16–111.
[2] R. Chhabra, "Nonwoven uniformity: measurements using image analysis," International Nonwovens Journal, vol. 12, no. 1, pp. 43–50, 2003, doi: 10.1177/1558925003os-1200112.
[3] B. Pourdeyhimi, L. Kohel, "Area-based strategy for determining web uniformity," Textile Research Journal, vol. 72, no. 12, pp. 1065–1072, 2002, doi: 10.1177/004051750207201205.
[4] E. Amirnasr, E. Shim, B.-Y. Yeom, B. Pourdeyhimi, "Basis weight uniformity analysis in nonwovens," J. Textile Institute, vol. 105, no. 4, pp. 444–453, 2014, doi: 10.1080/00405000.2013.820017.
[5] M. Godehardt, A. Moghiseh, C. Oetjen, J. Ohser, K. Schladitz, "An unambiguous cloudiness index for nonwovens," J. Math. Industry, vol. 12, 9, 2022, doi: 10.1186/s13362-022-00124-z.
[6] P. Moll, S. Wang, S. Coutandin, J. Fleischer, "Analysis of basis weight uniformity indexes for the evaluation of fiber injection molded nonwoven preforms," AUTEX Research Journal, vol. 21, no. 3, pp. 341–351, 2021, doi: 10.2478/aut-2020-0039.
[7] J.B. Carleton, A. D'Amore, K.R. Feaver, G.J. Rodin, M.S. Sacks, "Geometric characterization and simulation of planar layered elastomeric fibrous biomaterials," Acta Biomaterialia, vol. 12, pp. 93–101, 2015, doi: 10.1016/j.actbio.2014.09.049.
[8] S.H. Jeong, S.H. Kim, C.J. Hong, "The evaluation of evenness of nonwovens using image analysis method," Fibers and Polymers, vol. 2, no. 3, pp. 164–170, 2001, doi: 10.1007/BF02875331.
[9] M. Taşcan, S. Nohut, "Nondestructive prediction of areal weight, grab tensile strength and elongation at break of polypropylene spunbond nonwoven fabrics using digital image analysis," Tekstil ve Konfeksiyon, vol. 25, no. 1, pp. 24–32, 2015.